Development of high performance nanofibrous composite membranes by optimizing polydimethylsiloxane architectures for phenol transport

Meng-Yi Jin[1,2], Yuan Liao[1], Choon-Hong Tan[4], Rong Wang[*,1,3]

1. Singapore Membrane Technology Centre, Nanyang Environment and Water Research Institute, Nanyang Technological University, 1 Cleantech Loop, Singapore 637141, Singapore

2. Interdisciplinary Graduate School, Nanyang Technological University, 50 Nanyang Avenue, Singapore 639798, Singapore

3. School of Civil and Environmental Engineering, Nanyang Technological University, 50 Nanyang Avenue, Singapore 639798, Singapore

4. Department of Chemistry and Biological Chemistry, Nanyang Technological University, 21 Nanyang Link, Singapore 637371, Singapore

*Corresponding author at: School of Civil and Environmental Engineering, Nanyang Technological University, 639798 Singapore, Singapore.
Tel.: +65 6790 5327; fax: +65 6791 0676.
E-mail address: rwang@ntu.edu.sg (R. Wang).

Abstract

Phenol removal and recovery from wastewaters are highly demanded in industries due to its high toxicity and industrial importance. It can transport through the silicon-based rubber polydimethylsiloxane (PDMS) via the solution-diffusion mechanism. To improve the phenol removal efficiency in extractive processes, dense PDMS membranes with different macromolecular structures have been developed and evaluated in this work. The condensation-cured PDMS membranes (PA) with network architecture exhibited higher phenol partition coefficients (*K*) than the hydrosilylation-cured PDMS membranes with linear and branch architectures. This was attributed to the four-armed quaternary-siloxy linkages formed in the three-dimensional network structure, increasing the free volume for phenol passage and hydrogen bonding between phenol and PDMS matrix. The *K* of PA was further enhanced by optimizing the PDMS precursor chain length and cross-linker amount, and the corresponding membrane mechanical properties and phenol overall mass transfer coefficients (k_0) were examined. The optimal PA formulation was utilized to fabricate a highly effective nanofibrous composite membrane via spray coating. The resultant composite membrane exhibited a k_0 of 18.3 ± 1.3 x 10^{-7} m/s in an aqueous-aqueous extractive process, significantly outperforming the commercial counterpart with 45% increment. This is the first demonstration of the importance of PDMS macromolecular structures on phenol extraction. The newly-developed condensation-cured PDMS could contribute to the fabrication of highly effective composite membranes for various extractive processes.

Keywords: polydimethylsiloxane; phenol extraction; polymer architecture; nanofibrous composite membrane; spray coating

1. Introduction

Phenol and phenolic compounds exist widely in the effluents of many industries such as petrochemicals, textile, gas and coke manufactures, which are highly toxic to human and ecosystem due to their protein-degenerating effects and the formation of phenoxyl radicals [1, 2]. On the other hand, they are considered as valuable chemicals for producing polycarbonates, epoxies, nylon, detergents, herbicides and numerous pharmaceutical drugs [3]. Therefore, utilizing economically feasible and reliable technologies for efficient separation and recovery of phenol and phenolic compounds from wastewater streams before discharge is highly demanded. The technologies currently available for phenol treatment include: (1) traditional methods such as extraction [4], distillation [5], adsorption [6], biodegradation [7] and chemical oxidation [8]; (2) advanced methods such as photo oxidation processes [9] and membrane separation technologies [10]; and (3) hybrid systems which combine traditional and advanced techniques including reverse osmosis coupled with adsorption process [11], extractive membrane bioreactor (EMBR) [12-14], membrane aromatic recovery system (MARS) [15] and membrane pervaporation [16]. Among them, the hybrid systems employing membrane-based extractive processes, such as EMBR, have emerged as promising techniques [13, 14].

In the membrane-based aqueous-aqueous extractive processes, the target organic contaminants transport from the feed wastewaters to the receiving solutions through a dense membrane driven by the concentration gradient. As the feed and receiving solutions are separated by the membrane, the receiving solutions can have numerous options regardless of harsh conditions in the feed wastewaters. Additionally, the aqueous-aqueous extractive processe exhibits advantages including low energy consumption, low operating costs and

easy scalability [17, 18]. However, one of the main challenges in the aqueous-aqueous extractive processe is the shortage of specially designed membranes capable to extract the target organic compounds into the receiving aqueous medium with high efficiencies and excellent stabilities.

Owing to its organophilicity and hydrophobicity that allow preferential transfer of organics while rejecting water and inorganics, polydimethylsiloxane (PDMS) has been employed as the most commonly used membrane material in such configurations as silicone rubber tubes [17] and the selective layer of composite membranes [13, 14]. Small molecules can transport through the free volume of PDMS by the solution-diffusion mechanism, which involves three steps: adsorption at the upstream boundary, diffusion through the bulk membrane and desorption away from the downstream boundary [19]. The control of the adsorption, diffusion and desorption of the small molecules by engineering the polymer macromolecular structures, free volumes and functional groups to optimize mass transfer efficiency is of great value.

Generally, two types of cross-linking reaction pathways exist for PDMS preparation [20-22]. In the pathway of hydrosilylation reaction, a linear PDMS polymer structure can be formed by reacting vinyl-terminated PDMS precursors with hydrosilyl-containing cross-linkers under Pt catalysis; while in the condensation reaction pathway, hydroxyl-terminated PDMS precursors react with multi-functional cross-linkers under catalysis to generate a three-dimensional network [20-22]. Both methods have been adopted to fabricate PDMS-based membranes for applications such as gas separation [20], pervaporation [21] and solvent-resistant nanofiltration [22]. However, to the best of our knowledge, the effects of PDMS

cross-linking conditions and resultant polymer architectures on phenol transport behavior have not yet been studied systematically.

Additionally, the mechanical properties of the PDMS membrane are critical for practical applications, especially for the development of composite membranes. Although PDMS membranes have high organic affinity, they usually display unsatisfactory mechanical strength resulting from the intrinsic weak intermolecular interactions among the polymer chains [23] as well as the thin PDMS thickness (< 10 μm) for reducing the membrane resistance [14, 24]. Moreover, if the PDMS membranes are developed for pressure-driven processes such as gas separation, the mechanical strength needs to be further boosted so as to withstand the elevated pressure (> 100 bar) [25]. For the purpose of preparing high strength PDMS, a number of reinforcing fillers such as fumed silica and montmorillonite clays have been incorporated into the PDMS matrix [26-29]. However, pre-treatments such as surface modification of fillers [26, 28, 29] and functionalization of PDMS [27] are usually required in order to achieve adequate interfacial interactions between the fillers and PDMS matrix [29]. Alternatively, PDMS mechanical strength could be enhanced by optimizing the cross-linking methods and thus controlling the polymer architectures, which is considered to be more promising, convenient, economically valuable and practical [30]. However, the consequences of the architecture changes on the membrane separation performance, particularly, the phenol removal efficiency in extractive processes, have not been studied in details. Therefore, it is of high importance to systematically investigate the correlations among the cross-linking regimes, mechanical strength and phenol extractive performance of dense PDMS membranes.

Moreover, to meet the requirements of practical operations and enhance membrane permeability, an alternative option is to develop PDMS-based composite membranes by

means of coating a thin PDMS skin layer onto a highly porous substrate, which is capable of reducing the overall membrane resistance significantly [13, 14]. So far, the widely used membrane substrates are fabricated via phase inversion techniques, typically producing an asymmetric porous structure [31]. Our group has developed a series of electrospun nanofibrous membranes which exhibit highly porous and interconnected open structures, large surface area to volume ratio, controllable pore sizes and excellent tensile strengths, making them promising membrane substrates [13, 32]. Nevertheless, it is still challenging to directly form a thin and defect-free PDMS layer on the nanofibrous scaffolds as they usually possess large surface pore sizes (> 0.4 μm) [32].

To ensure the formation of defect-free selective layers, a stable and reproducible method to coat the PDMS layers on the nanofibrous substrates is essential [32]. Several coating methods have been reported in literatures to fabricate PDMS-based composite membranes: (1) dip coating is the most common approach to prepare the selective layer, but it is hard to produce a thin and uniform skin layer [33]; (2) spin coating is advanced to fabricate an ultrathin top selective layer, however the scalability of the process is limited [34]; (3) knife-coating (casting) method is a facile coating technique, and the membrane thickness could be controlled by adjusting the gap setting of the coating knife [35]; (4) spray coating has emerged as a versatile technique to produce a thin and uniform coating layer in a simple, fast and reproducible way [36]. In addition, the whole spray coating process can be conducted in an automatic manner which ensures the high reproducibility of this technique [36]. Thus, in this work, a spray coating technique was utilized to fabricate PDMS-coated nanofibrous composite membranes with high phenol mass transfer efficiency in an aqueous-aqueous extractive process.

In summary, both condensation and hydrosilylation reactions were adopted to prepare dense PDMS membranes with various polymer architectures. The corresponding PDMS structures were confirmed by ATR-FTIR and XPS analyses. Phenol partition coefficients of resultant dense PDMS membranes were examined. Moreover, PDMS precursor molecular weights as well as cross-linker amounts were varied to investigate their impacts on phenol partition efficiencies and mechanical strengths. Aqueous-aqueous phenol extractive tests were conducted to examine the phenol mass transfer efficiencies of selected dense PDMS membranes, from which the optimum conditions were identified to prepare the final composite membrane. An electrospun dual-layer polyvinylidene fluoride (PVDF) nanofibrous membrane with a tiered structure was utilized as the substrate to prepare PDMS-coated nanofibrous composite membranes. The morphologies of the resultant nanofibrous composite membranes were confirmed by FESEM and EDX. The phenol extractive performances of the composite membranes were examined in aqueous-aqueous phenol extractive tests.

2. Experimental

2.1. Materials and chemicals

Polyvinylidene fluoride (PVDF) (Kynar HSV900) supplied by Arkema was used as the substrate material. Anhydrous lithium chloride (LiCl, Merck chemicals) was added in polymer dope solutions as an additive. Vinyl-terminated polydimethylsiloxane (VPDMS, average molecular weight: 25000, viscosity: 850-1150 cSt), hydroxyl-terminated polydimethylsiloxane (HPDMS, viscosity: 750 cSt, 3500 cSt and 18000-22000 cSt, respectively), tetraethyl orthosilicate (TEOS), dibutyltin dilaurate (DBTDL), trimethylsilyl terminated poly(dimethylsiloxane-co-methylhydrosiloxane) (PDMS-MHS) and platinum(0)-

1,3-divinyl-1,1,3,3-tetramethyldisiloxane complex solution (Pt. catalyst, 0.05 M in vinyl terminated PDMS) were supplied by Sigma Aldrich. A two-component Sylgard® 184 silicone elastomer kit was supplied by Dow Corning. Acetone (Fisher Scientific), *n*-hexane (Merck chemicals) and N,N-dimethyl formamide (DMF, Merck chemicals) were used as solvents. Glycerol (85% aqueous solution, Merck chemicals) was mixed with deionized water (DI water, purified by a Milli-Q system, Millipore Co. Singapore) to prepare the substrate pre-wetting agent. Sodium chloride (Merck chemicals) and phenol (≥ 99%, Sigma Aldrich) were employed to prepare the feed solution. All the reagents were used directly without further treatment.

2.2. Preparation of dense PDMS membranes

To investigate the effect of polymer architectures on phenol extractive performances of dense PDMS membranes, three methods were used to prepare them. In the first method (condensation reaction), 10 wt% HPDMS was first dissolved and stirred in *n*-hexane at room temperature for 1 h. Desired amounts of cross-linker TEOS and catalyst DBTDL were added subsequently into the solution and stirred vigorously for 3 min. In order to identify the optimum formulation, HPDMS precursors with different molecular weights (reflected as viscosities: 750 cSt, 3500 cSt and 18000-22000 cSt) and TEOS with different amounts (3 wt%, 5 wt%, 10 wt% and 20 wt%) were used for the membrane preparation. The dense PDMS membrane fabricated by this method was denoted as PA. In the second method (hydrosilylation reaction), 10 wt% VPDMS and 3.5 wt% PDMS-MHS were dissolved and stirred in *n*-hexane at room temperature for 1 h, followed by adding 100 ppm Pt. catalyst. The dense PDMS membrane prepared by VPDMS and PDMS-MHS in the second method was named as PB. The PDMS prepared by commercial S184 kit method was chosen as a reference, which was designated as PK. In this kit method, 10 wt% vinyl-type PDMS

precursor was mixed with 1 wt% hydrosilyl-type cross-linker in *n*-hexane and stirred at room temperature for 1 h. For all methods, PDMS solutions were poured into Teflon moulds immediately after preparation. The complete evaporation of the solvent at room temperature followed by heat cure in an oven at 80 °C for 2 days resulted in the dense PDMS membranes.

2.3. Preparation of a tiered PVDF electrospun nanofibrous substrate

A dual-layer nanofibrous membrane with a tiered structure was fabricated by electrospinning as reported in our previous work [13]. Briefly, the nanofibrous substrate was prepared by electrospinning an 8 wt% PVDF dope solution to generate a coarse nanofibrous layer, on the top of which an ultrafine nanofibrous layer was fabricated by electrospinning a 3 wt% PVDF dope solution. In order to enhance the membrane mechanical strength and integrity, heat-press (Carver Inc, USA) post-treatment was carried out at 155 °C for 30 min. The post-treated nanofibrous substrate was then immersed sequentially in an 80 wt% ethanol aqueous solution, DI water and the pre-wetting agent (75 wt% glycerol aqueous solution) before the PDMS coating was conducted.

2.4. Preparation of nanofibrous composite membranes via spray coating

The PDMS-coated nanofibrous composite membranes were fabricated by spraying the PDMS solutions prepared by the condensation reaction or reference kit method onto nanofibrous substrate surfaces. An automatic spray coating machine (Model 7400, Spraying Systems Co., Singapore) was utilized to conduct the whole spraying process in a facile and reproducible manner. The coating solutions were injected via a syringe pump to an air atomizing nozzle through which the polymeric solutions were atomized and sprayed onto the horizontal-situated substrates. The coated membranes were dried in the open air for 30 min to evaporate the remaining solvent, and were then cured in an oven at 80 °C for two days in order to fully

cross-link the PDMS layer. The resultant PDMS-coated nanofibrous composite membranes were detached from the glass plate, and immersed in an 80 wt% ethanol aqueous solution for 10 min followed by DI water prior to evaluation.

2.5. Membrane Characterizations

A field emission scanning electron microscope (FESEM, JSM-7600F, JEOL Asia Pte Ltd, Japan) was used to observe the surface and cross-sectional morphologies of the membranes. The associated energy dispersive X-ray spectroscopy (EDX) equipment was employed to analyze the PDMS intrusion level into the substrates. The total membrane thickness was measured by a Vernier micrometer, while the top PDMS layer thickness of the nanofibrous composite membrane was estimated from the FESEM cross-sectional images. The chemical structures of the dense PDMS membranes were confirmed by a Fourier transform infrared (FTIR) spectrophotometer (IRPrestige-21 FTIR, Shimadzu, Japan) in attenuated total reflectance (ATR) mode with a resolution of 4 cm^{-1} and 45 scans. X-ray photoelectron spectroscopy (XPS: PHI Quantera II) with an Al Kα X-ray source was performed after 5 nm sputtering for the dense PDMS membrane samples to analyze the detailed membrane compositions, and the binding energy scale was calibrated by setting the C 1s core level peak at 284.8 eV [37]. The mechanical properties of the dense PDMS membranes were measured by a Zwick/Roell universal testing machine at room temperature.

2.6. Partition coefficient measurements

The partition coefficients of phenol between the aqueous phase and different dense PDMS membranes were measured according to the procedure reported in the literature [17]. Briefly, dense PDMS membranes with various volumes were soaked in different volumes of phenol solutions (200 ppm) in several containers. These containers were then put in a shaker for at

least 3 days until equilibria were reached. The partition coefficient K was given by the following equation:

$$C_0/C_{eq} - 1 = K * (V_m/V_f) \quad (1)$$

where V_f was the volume of phenol solution, V_m was the volume of dense PDMS membrane, C_0 was the initial phenol solution concentration, and C_{eq} was the phenol solution concentration at equilibrium. The plot of (C_0/C_{eq} – 1) against (V_m/V_f) provided a linear line with the partition coefficient K as the gradient.

2.7. Aqueous-aqueous extractive tests

The aqueous-aqueous phenol extractive tests were conducted for selected dense PDMS membranes and PDMS-coated nanofibrous composite membranes for 24 h [14]. The feed solution consisted of 1000 ppm phenol and 5 g/L NaCl in DI water while the receiving solution was DI water. The membranes were mounted into flat sheet membrane modules with an effective membrane area of 9 cm^2 for dense PDMS membrane and 36 cm^2 for nanofibrous composite membrane. The phenol mass transfer efficiency was characterized by overall mass transfer coefficient (OMTC) k_0 (m/s) which was calculated by the equation

$$k_0 = (\frac{dC_r}{dt} * V_r)/(A * (C_f - C_r)) \quad (2)$$

where C_r and C_f (g/m^3) were the phenol concentrations at receiving and feed sides, respectively, at time t (s), V_r (m^3) was the receiving solution volume, and A (m^2) was the effective membrane area. To examine membrane stability, a long-term aqueous-aqueous phenol extractive experiment was conducted for 2 weeks using the best nanofibrous composite membrane. The feed and receiving solutions were refreshed daily to maintain the same phenol concentration gradient during the long-term operation.

3. Results and discussion

3.1. Characterization of different dense PDMS membranes

The dense PDMS membranes are typically cross-linked from linear precursors, and their performances are intrinsically determined by respective chemical reaction. The cross-linking reactions conducted in this work and simplified schematic diagrams of the as-synthesized dense PDMS membranes are shown in **Fig. 1**. In the method for PA preparation (**Fig. 1A**), a condensation reaction was carried out between the hydroxyl-terminated PDMS precursor and the cross-linker TEOS with the aid of a catalyst DBTDL [21]. As depicted in **Fig. 1B**, the TEOS cross-linkers bridged the di-functional linear PDMS precursors as four-armed junction points, resulting in a three-dimensional network structure. Depending on the amount ratios between precursors and cross-linkers, the four active ethoxy groups in each TEOS could be fully or partially replaced by the hydroxyl-terminated PDMS precursors. In the method for synthesizing PB (**Fig. 1C**), the vinyl-terminated PDMS precursor reacted with the hydrosilyl-containing cross-linker under Pt catalysis through a hydrosilylation reaction pathway [38]. A linear structure linked by CH_2-CH_2 groups was obtained for PB as shown in **Fig. 1D**. According to the manufacturer information, the commercial S184 kit comprised a vinyl-type PDMS precursor and a hydrosilyl-type cross-linker [22]. Hence, it could be inferred that a hydrosilylation reaction similar to that for PB should be involved in the kit method. Structures including linear, branch or a combination of these two could exist in the kit-prepared PDMS membrane (PK) dictated by the exact formulation of the commercial kit.

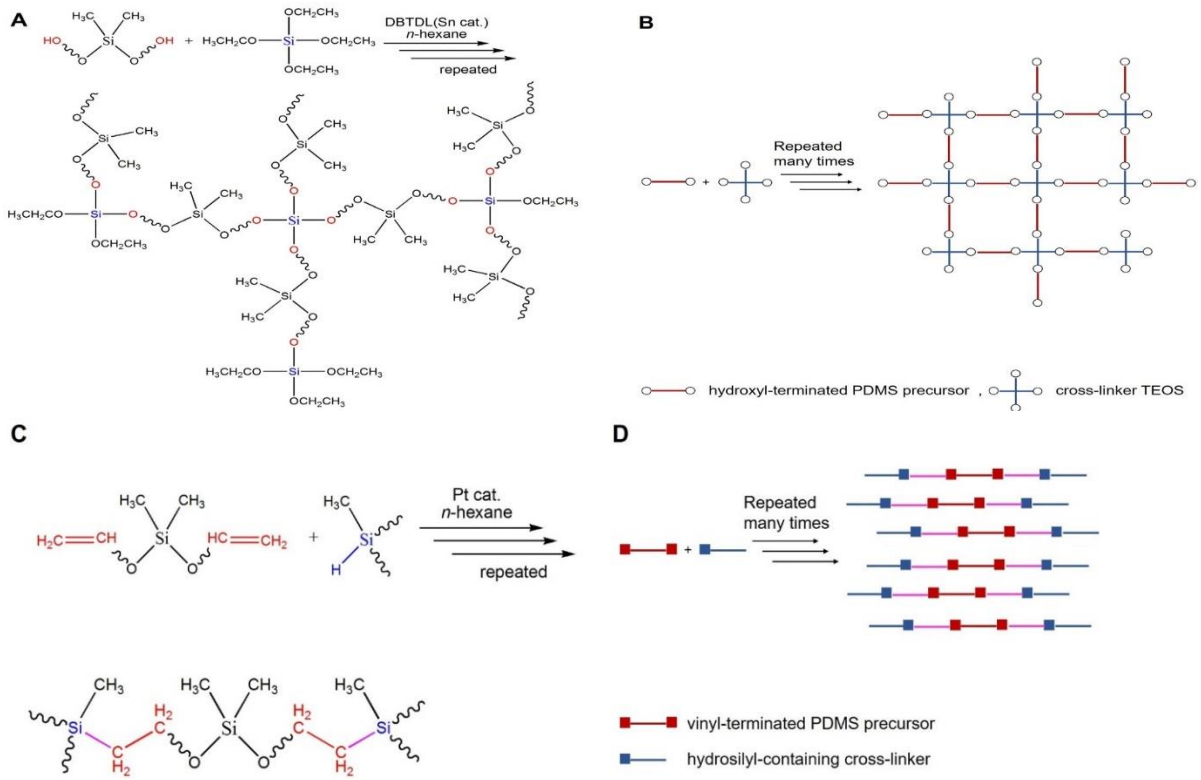

Fig. 1. Reaction pathways and schematic diagrams of the as-synthesized dense PDMS membranes PA (A and B) and PB (C and D).

The chemical structure characterizations of different dense PDMS membranes were performed by both ATR-FTIR and XPS. ATR-FTIR can provide qualitative information while XPS is well-suited to provide quantitative chemical analysis. All the as-developed dense PDMS membranes display similar ATR-FTIR spectra as presented in **Fig. 2**, which comply well with the literatures [39, 40]. The peak between 2950 and 2970 cm^{-1} corresponds to methyl stretching in Si-$(CH_3)_2$, while the methyl deformation vibration is observed in the range of 1400-1420 and 1245-1270 cm^{-1}. A broad and shouldered peak between 930 and 1200 cm^{-1} represents Si-O-Si asymmetric deformation. The Si-C band is found in the range of 825-865 cm^{-1}. In addition, a strong peak observed between 785 and 815 cm^{-1} corresponds to CH_3 rocking in Si-$(CH_3)_2$. The ATR-FTIR has demonstrated the successful cross-linking of the dense PDMS membranes.

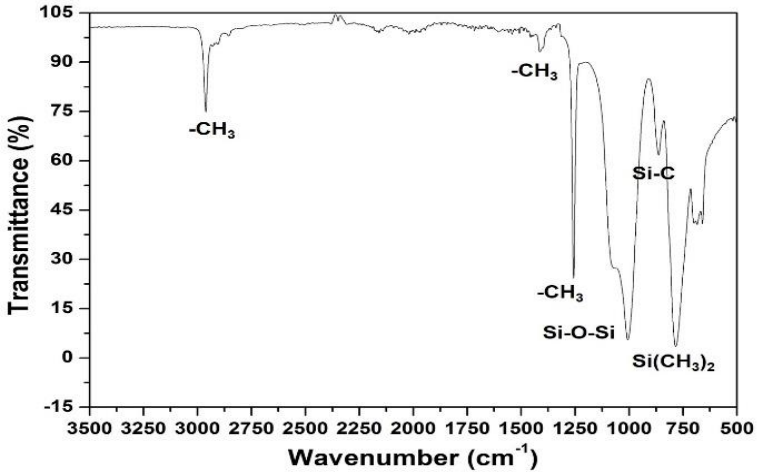

Fig. 2. ATR-FTIR spectrum of the dense PDMS membranes.

Fig.3 shows the XPS results, which analyze the chemical groups on PDMS surfaces in details. As shown in **Fig. 3A**, in a polysiloxane system, a silicon atom could exist in four kinds of chemical groups resulting in increasing Si binding energies with increasing oxygen atoms replacing the methyl groups [41, 42]. The chemical structures are denoted as M [mono-siloxy: $(CH_3)_3$-Si-$O_{1/2}$], D [di-siloxy: $(CH_3)_2$-Si-$O_{2/2}$], T [tri-siloxy: (CH_3)-Si-$O_{3/2}$] and Q [quaternary-siloxy: Si-$O_{4/2}$]. As a result, the Si 2p XPS spectrum of each PDMS membrane could be resolved into components corresponding to the chemical structures as presented in **Figs. 3B**, **3C** and **3D** [37, 41, 42].

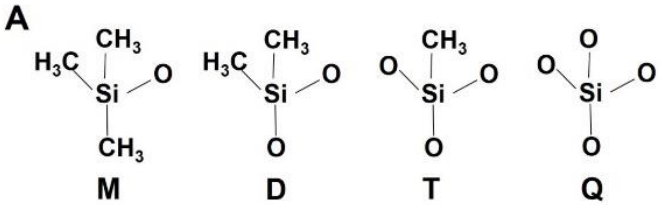

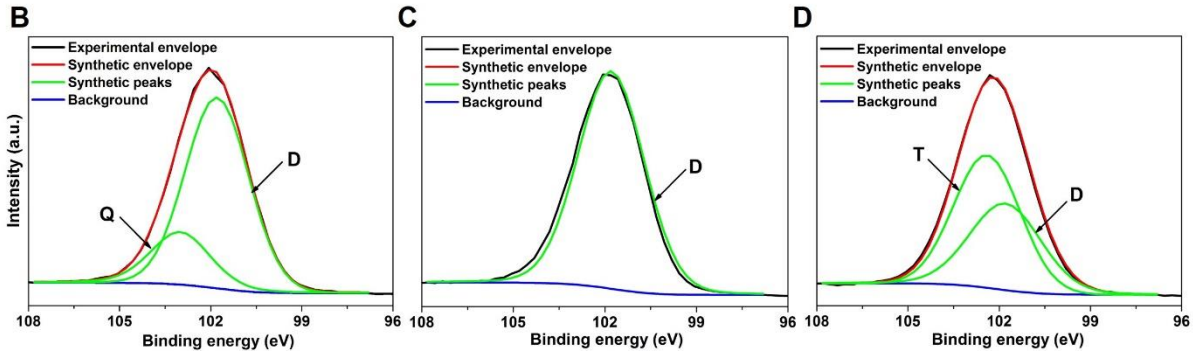

Fig. 3. (A) Chemical structures of the siloxy units present in polysiloxanes; Si 2p XPS spectra for the dense PDMS membranes: (B) PA, (C) PB and (D) PK.

As shown in **Fig. 3B**, the decomposed Si 2p XPS spectrum of PA contains a peak at 101.79 eV assigned to the D structure, corresponding to the dimethylsiloxane backbones of the PDMS membrane [37]. The Q structure presented at 103.00 eV demonstrates that the four-armed quaternary-siloxy units [Si-$O_{4/2}$] are formed as the linkages during the cross-linking reaction, confirming the three-dimensional network structure of PA as proposed in **Fig. 1B** [37]. In contrast, only the di-siloxy D structure is observed for the PDMS membrane PB (**Fig. 3C**), illustrating that a linear structure with dimethylsiloxane backbones is adopted by PB as shown in **Fig. 1D**. For the commercial PDMS membrane PK made via the kit method, both D and T structures (at 102.40 eV) exist (**Fig. 3D**) [37], implying that PK exhibits a chemical structure combining both linear and branch architectures. The presence of T structure should be ascribed to the fillers added in the kit formulation [22].

3.2. Phenol partition coefficients of dense PDMS membranes

A variety of mechanistic and phenomenological models have been proposed to explain the mass transfer behavior encountered in porous and dense membranes [43]. Regarding the dense membranes, the solution-diffusion model is the most popular one in which the solutes partition from the feed solutions into the polymeric bulk of the dense membranes, then

diffuse through the membrane bulk and are finally released into the permeate streams [14]. Most of the solute transport research does not take into account the solute partitioning rate into the polymeric dense membranes [43]. However, the phenol partition coefficient (*K*) has been identified as an essential parameter to determine the membrane mass transfer resistance [17].

In this work, the phenol partition coefficients of resultant dense PDMS membranes with different polymer architectures were examined at room temperature and pressure. As shown in **Fig. 4**, a linear partitioning of phenol into the dense PDMS membranes can be observed. The dense membrane PA with a three-dimensional network architecture exhibits the highest phenol partition coefficient (K = 1.145 ± 0.021), while the dense membrane PB with a linear structure obtains a K of 0.280 ± 0.013. Besides, the membrane PK with a combination of linear and branch architectures made by the S184 kit method shows a K of 0.322 ± 0.001. The phenol partition coefficient of PA exceeds that obtained from the commercial PK for over 3 times, revealing the significant improvement of phenol partition efficiency due to polymer macromolecular structure optimization.

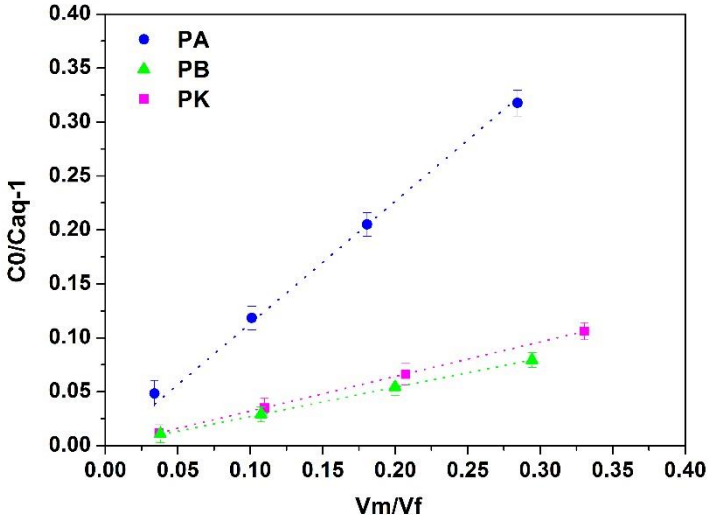

Fig. 4. Phenol partition coefficients (*K*'s, gradients of the linear lines) of dense PDMS membranes prepared with condensation reaction (PA), hydrosilylation reaction (PB) and commercial S184 kit method (PK).

The partition behavior of a given penetrant in a polymer matrix depends on the segmental mobility of the polymer chains, the free volume within the polymer and the interaction between polymer matrix and the compound, which are affected by the nature of polymer backbones, degree of cross-linking and crystallinity as well as the existence of substituent [44]. Thus the phenomenon of partition coefficient improvement could be explained by considering the respective polymer backbones and architectures (linear, branch and three-dimensional network) of the dense PDMS membranes, along with their siloxy group (Si-O) densities and corresponding interaction intensity (hydrogen bonding and Van der Waals force) with phenol molecules in a unit volume.

As illustrated in **Fig. 5A**, the dense membrane PA adopts a three-dimensional network structure with the four-armed quaternary-siloxy units as the junction points connecting the dimethylsiloxane backbones. The [Si-$O_{4/2}$] siloxy connection points are believed to be able to increase free volume available for the permeating molecules, resulting in an increase of phenol partition. Additionally, the [Si-$O_{4/2}$] siloxy units could offer extra interactions between the incoming phenol molecules and PDMS via hydrogen bonding, in addition to Van der Waals force provided by the dimethylsiloxane backbones [45, 46]. Moreover, these [Si-$O_{4/2}$] siloxy connection points produced by TEOS could cross-link to a large extent with themselves, leading to a much higher density of siloxy functional groups throughout the entire dense membrane [47]. Thus, all these effects synergistically enhance the affinity of phenol molecules towards the dense PDMS membrane PA.

On the contrary, the dense PDMS membrane PB is assumed to have a linear structure as a result of the hydrosilylation reaction pathway, where the polymer chains could arrange irregularly with respect to each other as shown in **Fig. 5B**. The substitution of the [Si-$O_{4/2}$] linkages by CH_2-CH_2 groups can dramatically reduce the permeability as a result of the increased polymer backbone rigidity and the decreased free volume available for the molecule diffusion [44]. The density of siloxy groups and corresponding intermolecular interactions between PDMS and phenol molecules are weakened as well [46], resulting in a much smaller phenol partition coefficient. The dense PDMS membrane PK prepared by the commercial kit method shows a slightly higher phenol partition coefficient than PB. This could be ascribed to the presence of the branch polymer structure, besides the linear structure (**Fig. 5C**). The branch polymer chains with tri-siloxy (T) groups can increase polymer free volume as well as hydrogen bonding available for phenol partition.

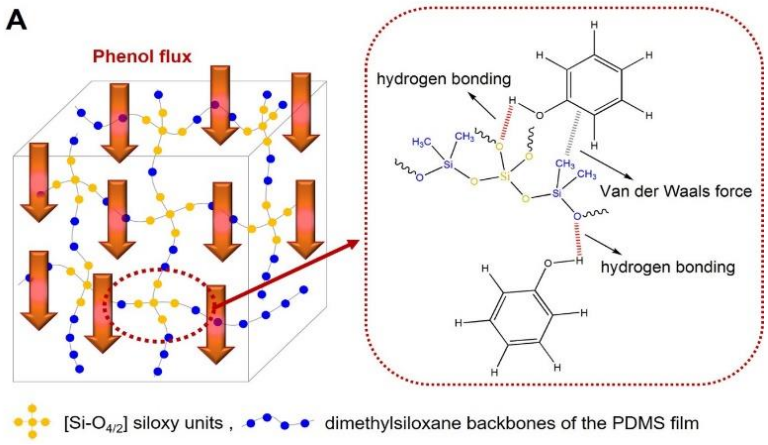

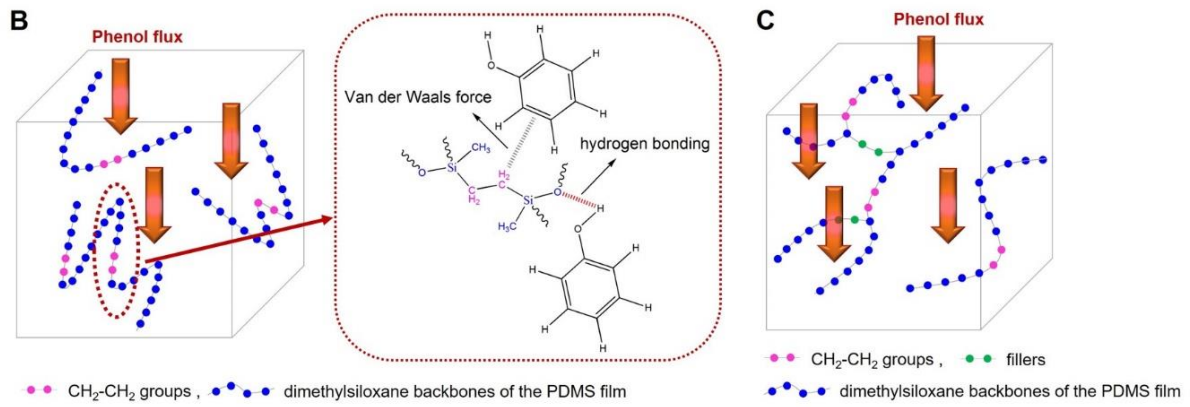

Fig. 5. Schematic diagrams showing phenol transport through PDMS unit volume and the primary interactions between phenol molecules and PDMS: (A) PA with network architecture, (B) PB with a linear architecture and (C) PK with a combination of linear and branch architectures.

3.3. Optimization of phenol partition coefficients of dense PDMS membranes

As a result of more free volumes and a higher density of functional siloxy groups, the dense PDMS membrane PA developed by condensation reaction has been proved to exhibit a higher phenol partition coefficient. It was reported that both PDMS precursor molecular weight and cross-link density could influence the molecular transport process [43]. Thus, in this part of work, the phenol partition coefficients of PA are further optimized by controlling PDMS precursor molecular weight and cross-linker amount.

It is presumable that the PDMS matrix cross-linked by polymer precursors with longer chains could possess a higher segmental mobility, thus more flexibility, own larger phenol transport channels and more free volumes, leading to higher partition for phenol molecules. When the PDMS precursor molecular weights are varied (**Fig. 6**), it turns out that only a slightly higher *K* value is obtained from the membrane fabricated from the high-mass precursor (denoted as PA-H, $K = 1.145 \pm 0.021$) than that from the low-mass precursor (denoted as PA-L, $K = 1.043 \pm 0.003$). These experimental results show that the improvement of phenol partition

efficiency by broadening transport channels and enhancing the free volume via increasing PDMS precursor molecular weights is negligible, largely due to the small molecular weight (94.1 g/mol) and volume (355 $Å^3$) of phenol [48].

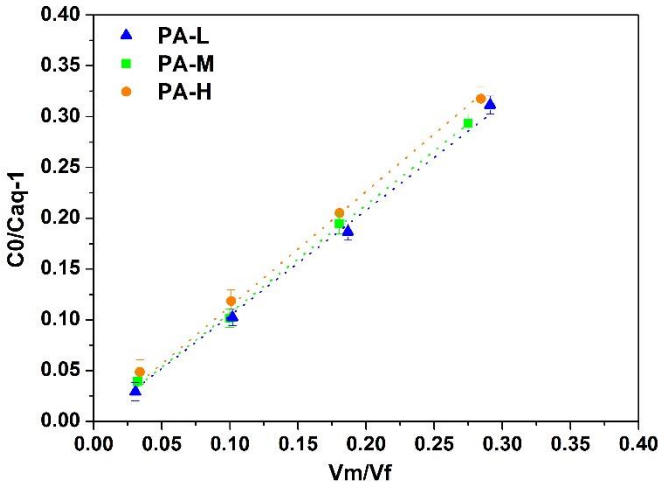

Fig. 6. Phenol partition coefficients (*K*'s, gradients of the linear lines) of dense PDMS membranes PA prepared with low-mass PDMS precursor (PA-L), middle-mass PDMS precursor (PA-M) and high-mass PDMS precursor (PA-H).

However, the phenol partition coefficients can be improved appreciably with the increase of cross-linker amounts as shown in **Fig. 7**. The dense PDMS membrane prepared from 20 wt% TEOS (denoted as PA-H-20) shows the highest *K* of 2.575 ± 0.041, while that from 3 wt% TEOS (denoted as PA-H-3) exhibits the lowest *K* of 1.011 ± 0.061. This result further emphasizes the importance of siloxy group on phenol partition efficiency of the resultant PDMS. As more four-armed junction points of quaternary-siloxy units are produced by increasing TEOS cross-linkers, it would lead to more functional units available for hydrogen bonding with phenol molecules.

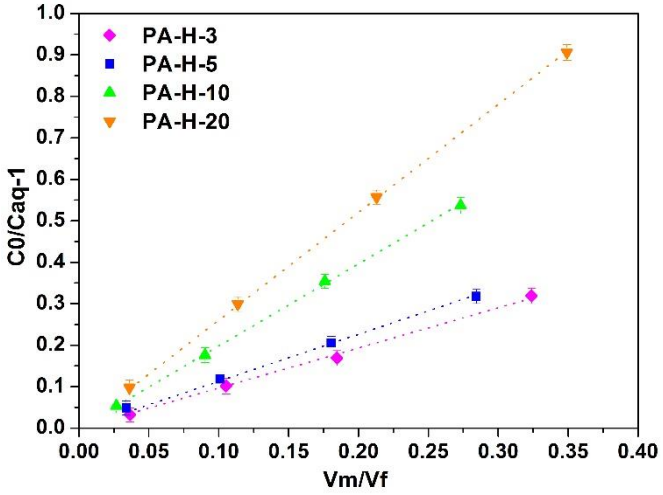

Fig. 7. Phenol partition coefficients (*K*'s, gradients of the linear lines) of dense PDMS membranes PA-H prepared with 3 wt% TEOS (PA-H-3), 5 wt% TEOS (PA-H-5), 10 wt% TEOS (PA-H-10) and 20 wt% TEOS (PA-H-20).

In order to confirm the polymer architectures of dense membranes PA prepared with different amounts of TEOS, the curve-fitted C 1s, O 1s and Si 2p XPS spectra of PA-H-5 and PA-H-20 are presented in **Fig. 8**. Both PDMS membranes PA-H-5 and PA-H-20 exhibit a single synthetic peak at 284.80 eV for the C 1s core level, as carbon atom is only present in the di-siloxy structure of PDMS (**Figs. 8A and 8B**) [37]. The same three-dimensional network polymeric architecture exists in both dense PDMS membranes PA-H-5 and PA-H-20, reflected by the presence of di-siloxy (D) and quaternary-siloxy (Q) components in the O 1s and Si 2p XPS spectra. As shown in **Figs. 8C** and **8D**, the O 1s core-level spectra of both PDMS membranes are decomposed to one peak at binding energy of 532.40 eV for the D unit and another peak at binding energy of 533.20 eV for the Q unit [37]. The structures can be further ascertained by the Si 2p core-level line shapes as shown in **Figs. 8E** and **8F**. A good fit to the analysis has been realized using O 1s and Si 2p core-level spectra. The intensities of the four-armed Q groups for PA-H-20 (**Figs. 8D** and **8F**) are higher than those for PA-H-5 (**Figs. 8C** and **8E**), demonstrating that a larger amount of [Si-$O_{4/2}$] siloxy units is obtained by adding more TEOS cross-linkers.

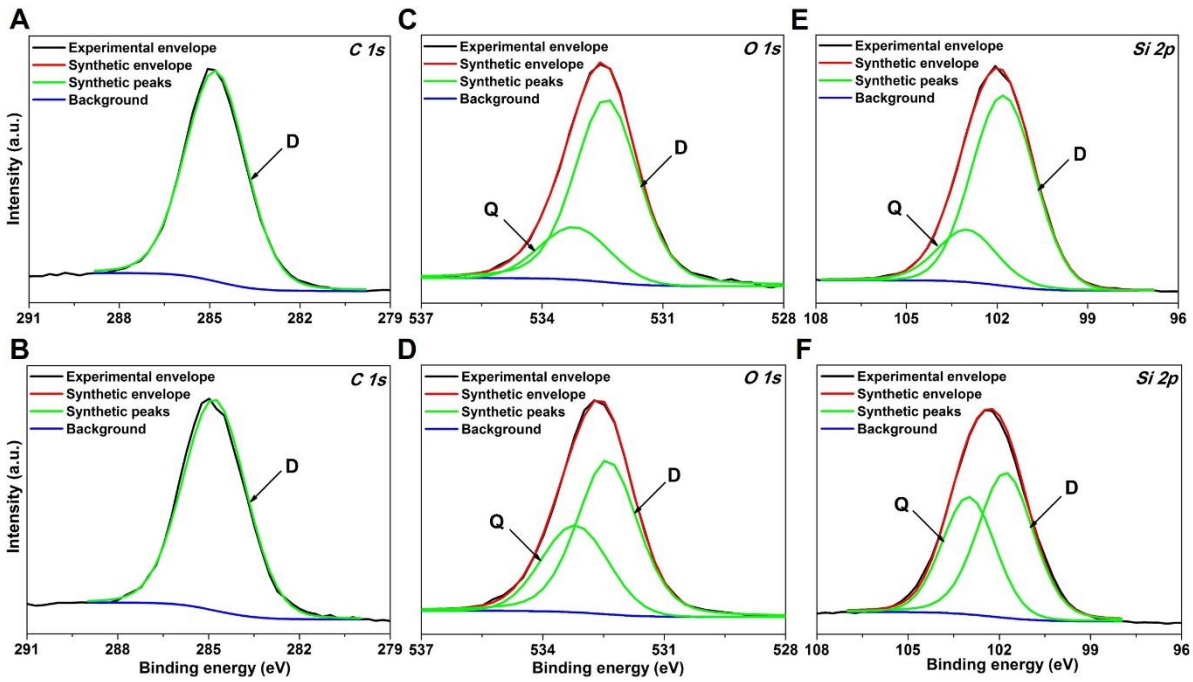

Fig. 8. C 1s, O 1s and Si 2p XPS spectra of dense PDMS membranes PA-H-5 (A, C and E) and PA-H-20 (B, D and F).

3.4. Mechanical properties of dense PDMS membranes

One limitation of dense PDMS membranes is the unsatisfactory mechanical properties. To fulfill the practical operation requirements, the mechanical strengths of dense PDMS membranes PA prepared in this work were evaluated as shown in **Fig. 9**. **Fig. 9A** illustrates the stress-strain curves for dense membranes PA prepared from PDMS precursors with different molecular weights. Two typical regions can be observed from the curves, including initial linear and second nonlinear regions: the initial linear region up to the proportional limit indicates the elastic behavior of PDMS and the tensile modulus is derived from the gradient of the linear portion based on Hooke's law, while the second nonlinear region represents strain hardening effect arising from stress-induced plastic deformation of the polymer chains [49, 50]. As shown in the **Fig. 9A**, the membranes become tougher with smaller precursor

molecular weights as the slopes of linear portions become higher. The highest tensile modulus (1.14 ± 0.05 MPa) and the lowest elongation at break (169.5 ± 7.1%) are observed for PA-L, as shown in **Figs. 9A** and **9B.** Whereas, the PA-H prepared by PDMS precursor with the highest molecular weight possesses the lowest tensile modulus (0.64 ± 0.02 MPa) and the highest elongation at break (251.2 ± 5.4%), indicating its best flexibility. This leads to a conclusion that a PDMS matrix utilizing the precursor with a lower molecular weight can be cross-linked more effectively, affording stiffer interaction and higher toughness.

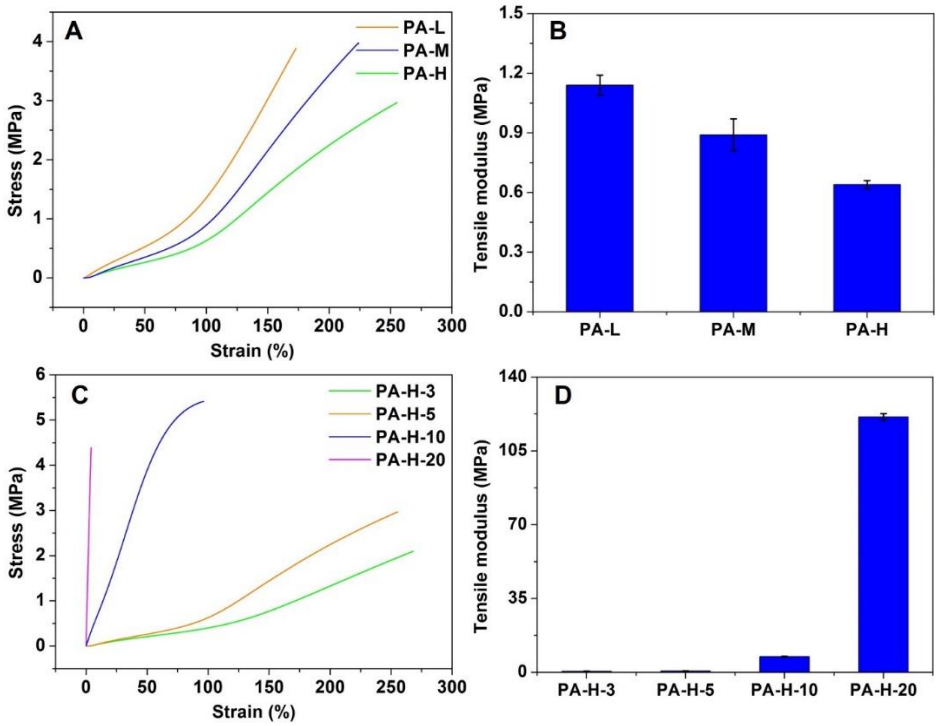

Fig. 9. Stress-strain curves and tensile moduli of the dense PDMS membranes PA prepared with different PDMS precursor molecular weights (A and B), and TEOS amounts (C and D).

Fig. 9C shows the effect of the cross-linker TEOS amounts on the mechanical properties of resultant dense PDMS membranes. The PA-H-20 exhibits a tensile modulus of 121.1 ± 1.5 MPa (**Fig. 9D**) with an increase of more than 200 times with respect to the PA-H-3. It demonstrates that a higher cross-linking degree attributed to increased cross-linker TEOS addition can endow the dense PDMS membrane with a greater mechanical robustness. The incorporation of TEOS replaces the weak polymer-polymer entanglement by the formation of

polymer-crosslinker-polymer covalent bonds. These tighter and more effective connections between polymer backbones lead to a more rigid polymer structure. Besides, the stress-strain curve of PA-H-20 shows a steep linear line in **Fig. 9C** over the full range of strain without appreciable plastic flow before fracture and possesses the lowest elongation of 4.0 ± 0.4%. The loss of flexibility is observed as a consequence of reducing mobility of the polymer chains. The stiffness enhancement with increasing TEOS amount could provide an important implication for design and development of strong PDMS materials in other applications.

3.5. Overall mass transfer efficiency of dense PDMS membranes

As stated earlier, in the solution-diffusion model, the permeating components desorb from the dense membrane into receiving streams after adsorption and diffusion through the membrane matrix. The removal of target components should be determined by the overall mass transfer efficiency combining the partition efficiency as well as the diffusion velocity. Thus, the three best dense PDMS membranes (PA-H-5, PA-H-10 and PA-H-20) based on the measurement of phenol partition coefficients and mechanical properties, along with the reference dense PDMS membrane PK, were tested in the aqueous-aqueous phenol extractive processes to obtain the overall mass transfer coefficient (k_0) of phenol. The dense PDMS membranes with thickness around 300 µm were fabricated. The k_0 of each dense PDMS membrane was tabulated in **Table 1**. All the PA membranes outperformed the reference dense PDMS membrane PK with over 50% higher k_0 values. This agreed well with the results from the phenol partition coefficient measurements. However, the k_0 values of the dense membranes PA prepared with different TEOS amounts did not differ much from each other, although their phenol partition coefficients varied. This phenomenon could be attributed to the low Reynolds number (270) applied during the operation, such that the liquid boundary layer resistances could dominate over the membrane resistance [17]. Consequently, the expected k_0

enhancement by increasing the quaternary-siloxy units was not fully revealed, leading to similar overall phenol mass transfer coefficients for the dense membranes PA prepared with different TEOS amounts. According to this result, 5 wt% TEOS was applied to prepare the final PDMS-coated nanofibrous composite membranes since the least amount of TEOS was sufficient to achieve high phenol extractive performance.

Table 1. Overall mass transfer coefficients, k_0, of selected dense PDMS membranes from aqueous-aqueous phenol extractive tests

Membrane	**Thickness (μm)**	k_0 **(E-07 m/s)**
PK	271 ± 45	1.54 ± 0.06
PA-H-5	291 ± 16	2.38 ± 0.02
PA-H-10	305 ± 10	2.23 ± 0.21
PA-H-20	299 ± 18	2.47 ± 0.21

3.6. Aqueous-aqueous extractive performance of nanofibrous composite membranes

To further reduce the membrane resistance for phenol transfer, the PDMS-coated nanofibrous composite membranes were designed and developed in this work. The FESEM images of the PVDF nanofibrous support with a tiered structure is shown in **Fig. 10**. It can be observed in **Fig. 10A** that the thickness of the top fine nanofiber layer is around 2.5 μm and that of the bottom coarse nanofiber layer is about 52 μm. Moreover, the delamination between the top ultrafine and the bottom coarse nanofibrous layers is not detected, confirming a good adhesion at the interface. As shown in **Figs. 10B** and **10C**, the average diameter of the nanofibers decreases from 148 ± 16 nm for the bottom coarse nanofibers to 72 ± 14 nm for the top ultrafine nanofibers, due to the enhancement of the dope conductivity and the reduction of dope concentration. This dual-layer nanofibrous substrate is designed to ensure a thin and defect-free PDMS coating layer and provide sufficient mechanical strength for practical operations [13].

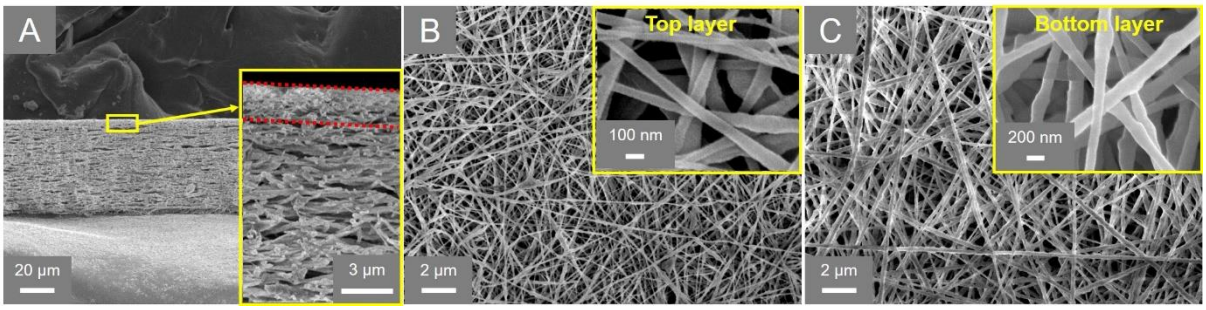

Fig. 10. (A) The cross sectional images of PVDF nanofibrous support with a tiered structure; the surface morphologies of (B) a top ultrafine PVDF nanofibrous layer and (C) a bottom coarse PVDF nanofibrous layer.

The spray coating method was utilized to fabricate a thin and uniform PDMS layer on the PVDF nanofibrous substrate. In order to mitigate PDMS intrusion into the substrate pores, the PDMS solutions with increased viscosity were prepared via a partially pre-crosslinking technique prior to spray coating [13]. The nanofibrous composite membrane coated by the PDMS solution prepared with the PA-H-5 formulation was denoted as M1, while the composite membrane coated by the PDMS solution prepared via the kit method was denoted as M2. By applying the same spray coating parameters, uniform and defect-free PDMS top selective layers were obtained for both nanofibrous composite membranes as observed in the FESEM surface images (**Figs. 11A1** and **11B1**). The thin PDMS layers had similar thicknesses of 7 µm (**Figs. 11A2** and **11B2**). Moreover, the elemental analyses for prepared nanofibrous composite membranes were carried out using EDX as shown in **Figs. 11A3-A4** and **11B3-B4**. The blue color denoted the presence of silicon element while the green color denoted the distribution of fluorine element, which were detected to identify the intrusion level of PDMS into PVDF nanofibrous substrates. It was found that, for both nanofibrous composite membranes M1 and M2, silicon was only observed on the substrate surfaces, rather than the bulk regions of the substrates. In other words, the intrusion of the top PDMS layers was mitigated effectively for both membranes.

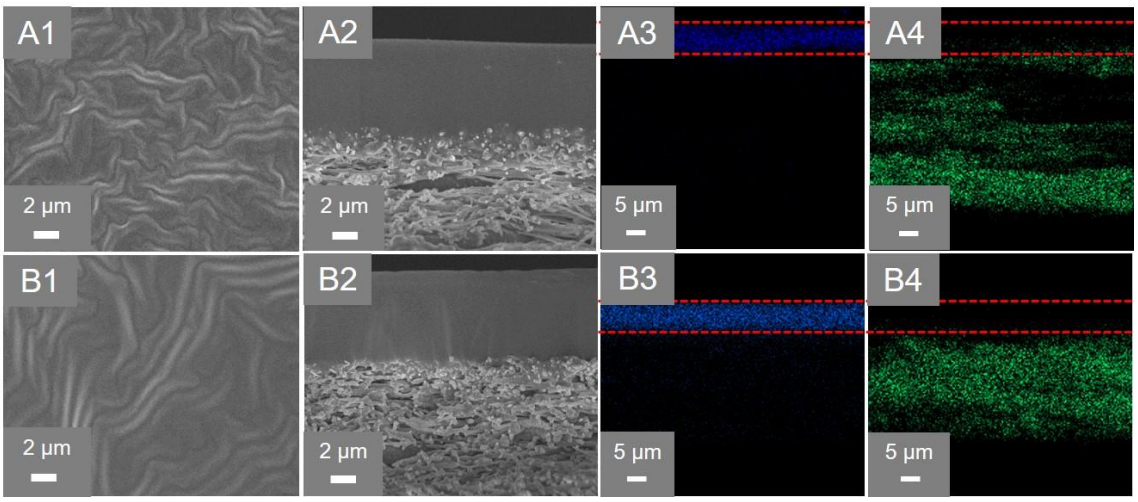

Fig. 11. Surface and cross-section FESEM images of PDMS-coated nanofibrous composite membranes M1 (A1 and A2) and M2 (B1 and B2); EDX images of PDMS-coated nanofibrous composite membranes M1 (A3 and A4) and M2 (B3 and B4) showing levels of PDMS intrusion into PVDF substrate pores, blue color denotes the presence of Si element, and green color denotes the presence of F element.

When the composite membranes were subjected to the aqueous-aqueous phenol extractive tests, M1 with an optimized PDMS coating layer developed in this work displayed a higher k_0 ($18.3 \pm 1.3 \times 10^{-7}$ m/s) than M2 coated with the commercial PDMS ($12.6 \pm 0.6 \times 10^{-7}$ m/s) as illustrated in **Table 2**. The significantly higher k_0 of membrane M1 should be attributed to the more efficient PDMS skin layer on the nanofibrous composite membrane surface. Additionally, salt flux was not detected for M1, revealing that the nanofibrous composite membrane spray-coated by the newly developed PDMS was defect-free and only allowed the partition and diffusion of phenol across the membrane during the extractive process.

Table 2. Aqueous-aqueous phenol extractive performances of PDMS-coated nanofibrous composite membranes.

Membrane Code	**PDMS preparation method**	**Top thickness (µm)**	**k_0 (E-07 m/s)**
M1	PA-H-5 formulation	7.1 ± 0.6	18.3 ± 1.3
M2	Kit method	6.9 ± 0.4	12.6 ± 0.6

Futhermore, the nanofibrous composite membrane M1 was continuously run in an aqueous-aqueous phenol extractive test for a total of 364 h to examine the membrane robustness and stability. As observed in **Fig. 12**, it performed steadily throughout the whole testing period and exhibited an average daily k_0 of 18.8 ± 0.2 x 10^{-7} m/s. In addition, insignificant NaCl flux (< 10 mg/m^2·h) was detected for the membrane M1, which demonstrated that M1 had stable structural integrity, giving rise to steady performance over a prolonged operation period.

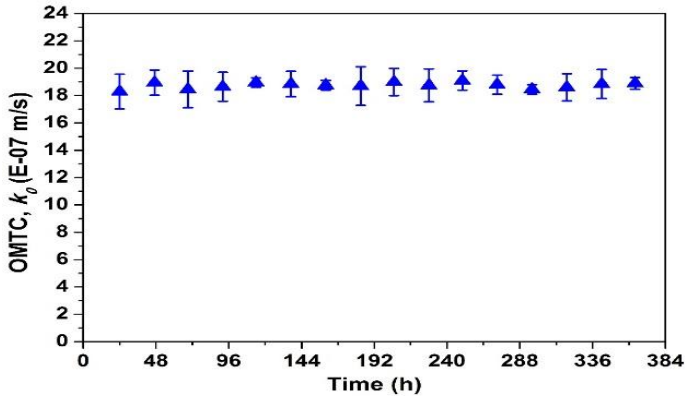

Fig. 12. Long term performance of the nanofibrous composite membrane M1.

The aqueous-aqueous phenol extractive performance of as-prepared nanofibrous composite membrane M1 was compared with that of a commercial tubular silicone rubber membrane [17], PDMS-coated thin film composite hollow fiber membranes [14, 51] and a PDMS-coated PVDF nanofibrous composite membrane developed in our previous study [13], as tabulated in **Table 3**. It could be seen that the composite membrane developed in this work outperformed most of the membranes reported in the literatures. One of the thin film composite hollow fiber membranes showed a higher performance, which could be due to a thinner PDMS selective layer. Compared with our previous nanofibrous composite membrane, the composite membrane developed in this work possessed a doubled k_0 due to a novel-developed thin and highly effective PDMS layer. The nanofibrous composite

membrane fabricated in this work can emerge as a promising membrane candidate to be utilized in extractive processes to remove phenol contaminants.

Table 3. Comparison of aqueous-aqueous phenol extractive performance of various membranes

Membrane	**PDMS thickness**	**Feed solution condition**	**Reynolds number**	**OMTC, k_0 (E-07 m/s)**
Tubular silicone rubber membrane [17]	0.5 mm	1000 ppm phenol solution	12000 (feed side) 4700 (receiving side)	1.0
Tubular silicone rubber membrane [17]	0.25 mm	1000 ppm phenol solution	12000 (feed side) 4700 (receiving side)	1.7
PDMS-PES TFC-HF membrane **[51]**	2 µm	phenol solution	7500 (feed side) 2700 (receiving side)	12
PDMS-PEI TFC-HF membrane [14]	0.5-2 µm	1000 ppm phenol, 50 g/L NaCl	1000 (both sides)	32
PDMS-PVDF nanofibrous composite membrane [13]	55 µm	1000 ppm phenol, 1 M HCl, 50 g/L NaCl	400 (both sides)	9.3
PDMS-PVDF nanofibrous composite membrane (this work)	7 µm	1000 ppm phenol, 5 g/L NaCl	270 (both sides)	18

4. Conclusions

In this work, three cross-linking reactions were adopted to prepare dense PDMS membranes with different polymer architectures. The condensation-cured membranes PA fabricated from hydroxyl-terminated PDMS precursors and TEOS cross-linkers exhibited a three-dimensional

network structure. The hydrosilylation-cured membrane PB with a linear architecture was prepared from a vinyl-terminated PDMS precursor and a hydrosilyl-type cross-linker, while the membrane PK with a linear and branch structure was developed by a commercial kit method. It was found that the four-armed quaternary-siloxy groups formed as the junction points in PA played a critical role in enhancing available free volume for phenol passage and affording additional hydrogen bonding between phenol and PDMS matrix, which contributed to a significant increase of phenol partition efficiency.

Additionally, the effects of PDMS precursor molecular weights and cross-linker amounts on the resultant PDMS membrane properties including phenol partition coefficient, mechanical strength and aqueous-aqueous phenol extractive performance were studied systematically. As phenol exhibited a small molecular size, the influence of broadening transport channels via lengthening the polymer chains on phenol partition was negligible. The phenol partition efficiency was improved greatly by increasing the cross-linker amount. High-mass PDMS precursor and 5 wt% TEOS used in the condensation reaction were found to be optimum considering the phenol partition coefficient, mechanical strength and aqueous-aqueous phenol extractive performance.

By employing the optimum PDMS preparation method, a highly efficient PDMS-coated nanofibrous composite membrane was fabricated via a spray coating technique. The overall mass transfer coefficient of the resultant membrane achieved a high value of $18.3 \pm 1.3 \times 10^{-7}$ m/s in the aqueous-aqueous extractive process. This surpassed the nanofibrous composite membrane coated by the commercial kit method with 45% increment. In addition, the as-developed nanofibrous composite membrane displayed a stable performance in a 2-week long-term operation with an average daily k_0 of $18.8 \pm 0.2 \times 10^{-7}$ m/s and insignificant NaCl

flux. This promising result demonstrated that the PDMS prepared by the optimized cross-linking condition could be utilized as a highly effective selective layer for composite membrane fabrication.

Acknowledgments

This research grant is supported by the Singapore National Research Foundation under its Environmental & Water Technologies Strategic Research Programme and administered by the Environment & Water Industry Programme Office (EWI) of the PUB (EWI RFP 1102-IRIS-02-03). We acknowledge funding support from the Singapore Economic Development Board to the Singapore Membrane Technology Centre (SMTC). We also appreciate the comments and advice provided by Professor Tony Fane from SMTC.

References

[1] I. Azni, S. Katayon, Degradation of phenol in wastewater using anolyte produced from electrochemical generation of brine solution, Global NEST Int. J., 4 (2002) 139-144.
[2] W. Kujawski, A. Warszawski, W. Ratajczak, T. Porebski, W. Capała, I. Ostrowska, Removal of phenol from wastewater by different separation techniques, Desalination, 163 (2004) 287-296.
[3] N. Rahmanian, S.M. Jafari, C.M. Galanakis, Recovery and removal of phenolic compounds from olive mill wastewater, J. Am. Oil Chem. Soc., 91 (2014) 1-18.
[4] K. Abbassian, A. Kargari, T. Kaghazchi, Phenol removal from aqueous solutions by a novel industrial solvent, Chem. Eng. Commun., 202 (2014) 408-413.
[5] P. Bartak, P. Frnkova, L. Cap, Determination of phenols using simultaneous steam distillation-extraction, J. Chromatogr. A, 867 (2000) 281-287.
[6] M.L. Soto, A. Moure, H. Domínguez, J.C. Parajó, Recovery, concentration and purification of phenolic compounds by adsorption: a review, J. Food. Eng., 105 (2011) 1-27.
[7] Y. Jiang, X. Cai, D. Wu, N. Ren, Biodegradation of phenol and *m*-cresol by mutated *Candida tropicalis*, J. Environ. Sci., 22 (2010) 621-626.
[8] S. Hamoudi, A. Sayari, K. Belkacemi, L. Bonneviot, F. Larachi, Catalytic wet oxidation of phenol over $Pt_xAg_{1-x}MnO_2/CeO_2$ catalysts, Catal. Today, 62 (2000) 379-388.
[9] S.J. Royaee, M. Sohrabi, Application of photo-impinging streams reactor in degradation of phenol in aqueous phase, Desalination, 253 (2010) 57-61.
[10] M.T.A. Reis, O.M.F. de Freitas, M.R.C. Ismael, J.M.R. Carvalho, Recovery of phenol from aqueous solutions using liquid membranes with Cyanex 923, J. Membr. Sci., 305 (2007) 313-324.
[11] A. Bódalo, J.L. Gómez, M. Gómez, G. León, A.M. Hidalgo, M.A. Ruíz, Phenol removal from water by hybrid processes: study of the membrane process step, Desalination, 223 (2008) 323-329.
[12] A.G. Livingston, A novel membrane bioreactor for detoxifying industrial wastewater: I. biodegradation of phenol in a synthetically concocted wastewater, Biotechnol. Bioeng., 41 (1993) 915-926.
[13] M.-Y. Jin, Y. Liao, C.H. Loh, C.-H. Tan, R. Wang, Preparation of polydimethylsiloxane–polyvinylidene fluoride composite membranes for phenol removal in extractive membrane bioreactor, Ind. Eng. Chem. Res., 56 (2017) 3436-3445.
[14] C.H. Loh, Y. Zhang, S. Goh, R. Wang, A.G. Fane, Composite hollow fiber membranes with different poly(dimethylsiloxane) intrusions into substrate for phenol removal via extractive membrane bioreactor, J. Membr. Sci., 500 (2016) 236-244.
[15] S. Han, F.C. Ferreira, A.G. Livingston, Membrane aromatic recovery system (MARS) -- a new membrane process for the recovery of phenols from wastewaters, Desalination, 188 (2001) 219-233.
[16] X. Hao, M. Pritzker, X. Feng, Use of pervaporation for the separation of phenol from dilute aqueous solutions, J. Membr. Sci., 335 (2009) 96-102.
[17] P.R. Brookes, A.G. Livingston, Aqueous-aqueous extraction of organic pollutants through tubular silicone rubber membranes, J. Membr. Sci., 104 (1995) 119-137.
[18] A. Splendiani, J. de Sa, R. Jorge, C. Nicolella, A.G. Livingston, K. Hughes, S. Cook, Development of an extractive membrane bioreactor for degradation of 3 chloro-4-methylaniline: from lab bench to pilot scale, Environmental Prog., 19 (2000) 18-27.
[19] J.G. Wijmans, R.W. Baker, The solution-diffusion model: a review, J. Membr. Sci., 107 (1995) 1-21.

[20] N. Bighane, W.J. Koros, Novel silica membranes for high temperature gas separations, J. Membr. Sci., 371 (2011) 254-262.
[21] J. Chen, J. Li, R. Qi, H. Ye, C. Chen, Pervaporation performance of crosslinked polydimethylsiloxane membranes for deep desulfurization of FCC gasoline I. effect of different sulfur species, J. Membr. Sci., 322 (2008) 113-121.
[22] L.E.M. Gevers, I.F.J. Vankelecom, P.A. Jacobs, Solvent-resistant nanofiltration with filled polydimethylsiloxane (PDMS) membranes, J. Membr. Sci., 278 (2006) 199-204.
[23] H. Cochrane, C.S. Lin, The influence of fumed silica properties on the processing, curing, and reinforcement properties of silicone rubber, Rubber Chem. Technol., 66 (1993) 48-60.
[24] L. Li, Z. Xiao, S. Tan, L. Pu, Z. Zhang, Composite PDMS membrane with high flux for the separation of organics from water by pervaporation, J. Membr. Sci., 243 (2004) 177-187.
[25] P. Bernardo, E. Drioli, G. Golemme, Membrane gas separation: a review/state of the art, Ind. Eng. Chem. Res., 48 (2009) 4638-4663.
[26] C.A. Dreiss, T. Cosgrove, N.J. Benton, D. Kilburn, M.A. Alam, R.G. Schmidt, G.V. Gordon, Effect of crosslinking on the mobility of PDMS filled with polysilicate nanoparticles: positron lifetime, rheology and NMR relaxation studies, Polymer, 48 (2007) 4419-4428.
[27] J. Ouyang, Y. Pan, S. Zhou, S.H. Goh, Supramolecular assembled C60-containing carboxylated poly(dimethylsiloxane) composites, Polymer, 47 (2006) 6140-6148.
[28] Q.G. Gu, Q.L. Zhou, Preparation of high strength and optically transparent silicone rubber, Eur. Polym. J., 34 (1998) 1727-1733.
[29] H. Takeuchi, C. Cohen, Reinforcement of poly(dimethylsiloxane) elastomers by chain-end anchoring to clay particles, Macromolecules, 32 (1999) 6792-6799.
[30] L.R.G. Treloar, The physics of rubber elasticity, 3rd ed., Clarendon, Oxford, UK, 1975.
[31] R.E. Kesting, Synthetic polymeric membranes, McGraw-Hill, NY, 1971.
[32] Y. Liao, R. Wang, M. Tian, C. Qiu, A.G. Fane, Fabrication of polyvinylidene fluoride (PVDF) nanofiber membranes by electro-spinning for direct contact membrane distillation, J. Membr. Sci. , 425-426 (2013) 30-39.
[33] B.K. Nandi, R. Uppaluri, M.K. Purkait, Effects of dip coating parameters on the morphology and transport properties of cellulose acetate–ceramic composite membranes, J. Membr. Sci., 330 (2009) 246-258.
[34] C.A. Page, A.E. Fouda, T. Matsuura, Pervaporation performance of polyetherimide membranes spin- and dip-coated with polydimethylsiloxane, J. Appl. Polym. Sci., 54 (1994) 975-989.
[35] Y. Chen, W.S.W. Ho, High-molecular-weight polyvinylamine/piperazine glycinate membranes for CO2 capture from flue gas, J. Membr. Sci., 514 (2016) 376-384.
[36] H. Fan, Q. Shi, H. Yan, S. Ji, J. Dong, G. Zhang, Simultaneous spray self-assembly of highly loaded ZIF-8-PDMS nanohybrid membranes exhibiting exceptionally high biobutanol-permselective pervaporation, Angew. Chem. Int. Ed., 53 (2014) 5578-5582.
[37] J.F. Moulder, W.F. Stickle, P.E. Sobol, K.D. Bomben, Handbook of X-ray photoelectron spectroscopy, ULVAC-PHI, Inc., Japan and Physical Electronics USA, Inc., United States of America, 1992, 1995.
[38] T.R.E. Simpson, B. Parbhoo, J.L. Keddie, The dependence of the rate of crosslinking in poly(dimethyl siloxane) on the thickness of coatings, Polymer, 44 (2003) 4829-4838.
[39] K. Berean, J.Z. Ou, M. Nour, K. Latham, C. McSweeney, D. Paull, A. Halim, S. Kentish, C.M. Doherty, A.J. Hill, K. Kalantar-zadeh, The effect of crosslinking temperature on the permeability of PDMS membranes: evidence of extraordinary CO2 and CH4 gas permeation, Sep. Purif. Technol., 122 (2014) 96-104.
[40] D. Bodas, C. Khan-Malek, Formation of more stable hydrophilic surfaces of PDMS by plasma and chemical treatments, Microelectron. Eng., 83 (2006) 1277-1279.

[41] L.-A. O'Hare, A. Hynes, M.R. Alexander, A methodology for curve-fitting of the XPS Si 2p core level from thin siloxane coatings, Surf. Interface Anal., 39 (2007) 926-936.
[42] L.-A. O'Hare, B. Parbhoo, S.R. Leadley, Development of a methodology for XPS curve-fitting of the Si 2p core level of siloxane materials, Surf. Interface Anal., 36 (2004) 1427-1434.
[43] J. Wang, D.S. Dlamini, A.K. Mishra, M.T.M. Pendergast, M.C.Y. Wong, B.B. Mamba, V. Freger, A.R.D. Verliefde, E.M.V. Hoek, A critical review of transport through osmotic membranes, J. Membr. Sci., 454 (2014) 516-537.
[44] S.C. George, S. Thomas, Transport phenomena through polymeric systems, Prog. Polym. Sci., 26 (2001) 985-1017.
[45] J.D. Plessis, W.J. Pugh, A. Judefeind, J. Hadgraft, The effect of hydrogen bonding on diffusion across model membranes: consideration of the number of H-bonding groups, Eur. J. Pharm. Sci., 13 (2001) 135-141.
[46] C. Nagel, K. Günther-Schade, D. Fritsch, T. Strunskus, F. Faupel, Free volume and transport properties in highly selective polymer membranes, Macromolecules, 35 (2002) 2071-2077.
[47] M. Bennett, B.J. Brisdon, R. England, R.W. Field, Performance of PDMS and organofunctionalised PDMS membranes for the pervaporative recovery of organics from aqueous streams, J. Membr. Sci., 137 (1997) 63-88.
[48] A. Dąbrowski, P. Podkościelny, Z. Hubicki, M. Barczak, Adsorption of phenolic compounds by activated carbon—a critical review, Chemosphere, 58 (2005) 1049-1070.
[49] I.D. Johnston, D.K. McCluskey, C.K.L. Tan, M.C. Tracey, Mechanical characterization of bulk Sylgard 184 for microfluidics and microengineering, J. Micromech. Microeng., 24 (2014) 035017.
[50] M. Liu, J. Sun, Y. Sun, C. Bock, Q. Chen, Thickness-dependent mechanical properties of polydimethylsiloxane membranes, J. Micromech. Microeng., 19 (2009) 035028.
[51] U. Cocchini, C. Nicolella, A.G. Livingston, Countercurrent transport of organic and water molecules through thin film composite membranes in aqueous-aqueous extractive membrane processes. part I: experimental characterisation, Chem. Eng. Sci., 57 (2002) 4087-4098.